Journal of Catalysis 294 (2012) 79–88

Contents lists available at SciVerse ScienceDirect

Journal of Catalysis

journal homepage: www.elsevier.com/locate/jcat

In situ study of activation and de-activation of LSM fuel cell cathodes – Electrochemistry and surface analysis of thin-film electrodes

Anne-Katrin Huber [a], Mareike Falk [a], Marcus Rohnke [a], Bjoern Luerssen [a], Matteo Amati [b,1], Luca Gregoratti [b,1], Dietrich Hesse [c,2], Jürgen Janek [a,*]

[a] Institute of Physical Chemistry, Justus-Liebig University, 35392 Gießen, Germany
[b] Sinchrotrone Elettra, 34012 Basovizza-Triestes, Italy
[c] Max Planck Institute of Microstructure Physics, 06120 Halle, Germany

ARTICLE INFO

Article history:
Received 14 May 2012
Revised 6 July 2012
Accepted 10 July 2012
Available online 17 August 2012

Keywords:
SOFC cathode
LSM
Polarization
In situ XPS
In situ SIMS

ABSTRACT

The activation mechanism of the (ORR) on lanthanum strontium manganite (LSM) thin-film electrodes is investigated by examining the electrochemical behavior with impedance spectroscopy. To clarify whether surface segregation processes induced by electrochemical polarization are responsible for the change in catalytic activity of the perovskite electrode, in situ investigations with X-ray photoelectron spectroscopy (XPS) and static secondary ion mass spectrometry (SIMS) were performed. The surfaces of the as-prepared thin-film electrodes, which were annealed at elevated temperatures during the preparation process, show an increased strontium surface concentration. The segregated SrO surface layer has a detrimental effect on the ORR reaction. Cathodic polarization decreases the strontium surface concentration while anodic polarization causes strontium accumulation at the electrode surface, which is proven by both SIMS and XPS in situ. A mechanism based on the incorporation of poorly conductive SrO from the electrode surface into the LSM lattice under cathodic polarization is suggested to be responsible for the observed activation process.

1. Introduction

Solid Oxide Fuel Cells (SOFCs) are electrochemical devices that convert chemical energy of fuels like petroleum, diesel, or natural gas into electrical energy with very high efficiency. In the last decades, they have attracted a lot of attention as sources of electricity with comparably low emissions. A detailed review of SOFC techniques and the SOFC operation principle is given by Minh and Minh [1].

Commonly used materials are $La_{0.8}Sr_{0.2}MnO_3$ (LSM) cathodes due to their excellent electronic conductivity and good catalytic activity toward the oxygen reduction reaction (ORR), Y_2O_3-stabilized ZrO_2 (YSZ) as solid electrolyte, and Ni/YSZ cermet anodes.

Sr-doped $LaMnO_3$ is commonly used as cathode material because it provides good electrical and ionic conductivity at elevated temperatures, good thermal and chemical compatibility with YSZ, and relatively high catalytic activity for the ORR. However, the low oxygen-ion conductivity limits the operation temperature to above 800 °C [2]. Much effort has been spent to reduce the operation temperature. As a result improved perovskite-type cathode materials have been reported, highlighting the structural flexibility of the perovskite lattice that tolerates different dopants and allows to tailor the electrode properties to a certain extent – but leading to complex solid solutions.

An interesting step to enhance the catalytic activity of a given cathode is the application of an initial cathodic current. For example, Jiang and Love [3] reported that the ORR overpotential of a porous screen-printed $(La_{0.8}Sr_{0.2})_{0.9}MnO_3$ electrode was reduced from initially 290 mV to 80 mV by applying a cathodic current of 500 mA cm^{-2} at 1000 °C for 30 min. Similar results were also reported by other authors [4,5].

Activation phenomena are well known in heterogeneous catalysis and have also often been reported for metallic electrodes like platinum during electrochemical polarization [6–8]. For Pt electrodes, the activation process is explained by the decomposition of passivating PtO_x surface and interface films under cathodic polarization [6,8,9]. For LSM electrodes as quaternary phases, the situation is much more complex and less is known about the mechanism of the electrochemical activation under cathodic current treatment.

Several authors have proposed different models to explain the activation step. In brief, the catalytic activity improvement under cathodic polarization is attributed to (a) either the partial reduction of Mn(III) to Mn(II) with simultaneous generation of oxygen

* Corresponding author. Fax: +49 6419934509.
E-mail addresses: luca.gregorattix@elettra.trieste.it (L. Gregoratti), hesse@mpi-halle.de (D. Hesse), Juergen.Janek@phys.chemie.uni-giessen.de (J. Janek).
[1] Fax: +39 0403758565.
[2] Fax: +49 3455511223.

0021-9517/$ - see front matter © 2012 Elsevier Inc. All rights reserved.
http://dx.doi.org/10.1016/j.jcat.2012.07.010

vacancies, finally leading to improved oxygen ion transport [10,11], (b) microstructural and morphological changes at the LSM/YSZ interface and at the surface, and in consequence improved oxygen diffusion kinetics [12–14], (c) the removal or incorporation of poorly conductive surface layers like SrO and MnO_x, which inhibit surface oxygen exchange kinetics [15], and (d) the extension of the active area for O_2 reduction by spreading of Mn(II) onto the electrolyte surface and direct incorporation of oxygen into the electrolyte at the catalytically modified electrolyte surface [16].

The reduction of Mn(III) to Mn(II) with simultaneous generation of oxygen vacancies was observed by X-ray photoelectron spectroscopy (XPS) and ultraviolet photoelectron spectroscopy (UPS) [17,18], but it is still not proven whether this reduction process occurs also under ambient pressure.

Morphological and structural changes after cathodic polarization were investigated by X-ray diffraction (XRD), high-resolution scanning electron microscopy (HSEM), and transmission electron microscopy (TEM), but these microstructural changes can hardly explain the large magnitude of the observed electrochemical activation [19].

Other studies showed that cathodic polarization is accompanied by significant changes of cation surface concentrations. For example, Backhaus-Ricoult et al. [16] proposed a mechanism with direct incorporation of oxygen from the gas phase into the electrolyte due to a strong enrichment of Mn(II) at the electrolyte surface induced by cathodic polarization.

A decrease in surface La concentration and increased Sr and Mn fractions at the three-phase boundary (TPB) under cathodic polarization were demonstrated by La O' et al. [20,21]. The removal of inhibiting La species leads to the formation of Sr-enriched LSM and oxygen-deficient $Sr_xMn_yO_z$ particles at the TPB with enhanced oxygen permeability and electrical conductivity.

However, the results are in disagreement with the work of Wang and Jiang [15] who proposed a mechanism that involves the incorporation of inhibiting SrO species into the LSM lattice under cathodic polarization, thereby facilitating the oxygen surface exchange reaction, resulting in the observed electrochemical activation.

An alternative explanation was proposed by Vance and McIntosh [22]. They compared the activation behavior of pure LSM electrodes with Mn, Sr, and La surface-doped electrodes. The Sr-doped electrodes show an activation behavior according the results of Wang and Jiang [15] and support the concept of inhibiting SrO surface species. But the activation behavior was removed by La surface-doped electrodes, suggesting that La species play an important role in the activation mechanism.

Evidence of Sr surface enrichment on freshly prepared LSM electrodes has been reported in different studies by XPS, Auger electron spectroscopy (AES) and low energy ion scattering (LEIS). Decorse et al. [23] were first to demonstrate higher Sr surface concentrations relative to the bulk composition on $La_{1-x}Sr_xMnO_{3\pm\delta}$ electrodes indicating SrO surface segregation. Sr segregation upon heat treatment was reported by Wu et al. [24]. They found small amounts of SrO on the LSM surface after heat treatment under UHV condition at 600 °C. But a direct evidence for surface chemical composition changes induced by electrochemical polarization is still missing.

Therefore, we focused our experiments on the in situ observation of surface composition changes induced by electrochemical polarization. We prepared well-defined thin-film model electrodes with pulsed laser deposition (PLD) to achieve a reasonably defined surface area and TPB length. The improvement of the electrochemical performance of LSM electrodes under cathodic polarization was studied by electrochemical impedance spectroscopy (EIS). The observed activation is strongly accompanied by surface composition changes; therefore, in situ XPS and scanning photoelectron spectroscopy (SPEM) and static secondary ion mass spectrometry (SIMS) were used to monitor the effect of electrochemical polarization on the surface composition of the electrodes. The spectroscopic measurements have been performed at reduced pressure; thus, in comparison with observations at atmospheric pressure, one has to take the "pressure gap" into account. However, as the spectroscopic experiments are performed "live" during the electrochemical experiment, we retain the term in situ. Microstructural and morphological investigations of the freshly prepared LSM electrodes and of such after cathodic and anodic polarization, respectively, were performed by plan-view HSEM and cross-sectional TEM.

2. Experimental

2.1. Sample preparation

Square thin-film electrodes with an area of 1 cm^2 were deposited through a stainless steel mask on YSZ (1 1 1) single crystalline substrates (8 mol% Y_2O_3) (*CrysTec*, *Germany*) by PLD.

$(La_{0.8}Sr_{0.2})_{0.92}MnO_3$ was prepared by the citrate complex sol–gel route. Stoichiometric amounts of $La(NO_3)_3{\cdot}6H_2O$ (99% *ChemPur*) and $Sr(NO_3)_2$ (99% *Alfa Aesar*) were dissolved in ethylene glycol. The mixed nitrate solution was added to a mixture of $MnN_2O_6{\cdot}4H_2O$ (98% *Alfa Aesar*), citric acid, and ethylene glycol in the ratio 1:4:3.99. The solution was stirred and heated up to 90 °C for 1 h. For further concentration, the mixture was heated up to 150 °C then forming a homogeneous brown gel, which was finally calcinated at 600 °C for 5 h.

The powder was characterized by XRD and inductively coupled plasma mass spectrometry (ICP-MS) to verify the formation of the $(La_{0.8}Sr_{0.2})_{0.92}MnO_3$ perovskite phase (see Supporting information).

The calcined powder was wet milled in isopropanol, isostatically pressed into pellets and sintered at 800 °C for 3 h. The sintered pellets were used as targets for the laser ablation process.

For the PLD process, a KrF excimer laser with a wave-length of 248 nm was used. The laser power was fixed at 300 mJ/pulse with a pulse frequency of 5 Hz. The oxygen partial pressure in the chamber was held constant at 1×10^{-2} mbar in order to avoid film cracking, and the temperature of the substrate was 450 °C during the deposition for 60 min. The as-grown films were annealed at 800 °C for 3 h in an oxygen atmosphere to obtain the perovskite phase. The samples were characterized by XRD and HSEM (see Supporting information).

2.2. Electrochemical setup

Polarization measurements were performed in a two-electrode arrangement (Fig. 1) with a porous Pt counter electrode (CE) symmetrically arranged opposite to the working electrode (WE) to minimize errors in electrochemical measurements [25,26]. EIS

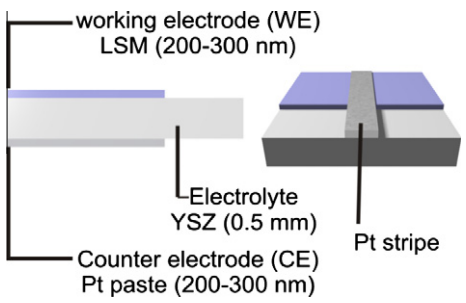

Fig. 1. Schematic diagram of the cell configuration for the two-electrode measurements used in this study.

measurements were performed without bias potential within the frequency range from 0.1 Hz to 10 kHz and a signal amplitude of 10 mV with a VersaStat3.400 potentiostat frequency analyzer (*Princeton Applied research*). The electrode area was $1 \times 1\ cm^2$. The polarization experiments were started by applying a constant cathodic potential of −2.5 V for different periods at 800 °C. The electrode resistance R was determined directly by the difference of the high- and low-frequency intercept with the real axis from the impedance data.

2.3. In situ XPS

High-resolution XPS and SPEM were performed at the ESCA microscopy beamline at the ELETTRA synchrotron light facility in Trieste, Italy [27–29]. For the polarization experiments, the samples were heated in the ESCA chamber up to 600 °C in an oxygen partial pressure of 10^{-6} mbar. The XPS and SPEM measurements were carried out with the Sr 3d, Mn 3p, and La 4d spectral lines. The binding energy scale was adjusted by the position of the Fermi level to compensate possible changes due to the electrochemical polarization. After Shirley type background correction, the spectra were fitted by using the XPSPeak4.0 software. The experimental set-up is depicted in Fig. 2. More experimental details are given in Supporting information.

2.4. Quasi in situ SIMS

For SIMS measurements, a TOF.SIMS5 spectrometer (IonTOF, Münster, Germany) was used. A detailed explanation of the used SIMS technique is given in Supporting information. The experimental set-up is depicted in Fig. 3. The LSM samples were heated up to 500 °C in the SIMS chamber with an oxygen partial pressure of 10^{-6} mbar. The polarization potentials were applied by a Keithley 2004 SourceMeter, and after continuous polarization for 30 min, the samples were quickly cooled down (the interruption for cooling down, image uptake, and reheating took approximately 20 min) to minimize the background in the SIMS spectra, and then, the measurements were performed. Successive heating/polarization/cooling cycles were performed in order to check the reproducibility of the experiments. All spectra and images were standardized and analyzed with the ToF-SIMS software V4.1 (IonImage and IonSpectra).

2.5. Morphological and microstructural investigations by HSEM and TEM

Morphology and microstructure of freshly prepared LSM electrodes and of such after cathodic and anodic polarization, respectively, were investigated by HSEM and TEM. For HSEM, a scanning electron microscope of type LEO Gemini 982 was applied. TEM investigations were performed by a Philips CM20Twin microscope at an energy of the primary electrons of 200 kV, applying diffraction contrast to suitably thinned cross-section samples. The latter were prepared by state-of-the-art mechanical and ion-beam methods, in particular using a Gatan Precision Ion Beam Polishing System (PIPS).

3. Results and discussion

3.1. Electrochemical impedance spectroscopy

3.1.1. Cathodic polarization

The impedance response of a freshly prepared LSM electrode on YSZ (1 1 1) (Fig. 4, black dots) was significantly reduced by 15% only by applying a cathodic potential of −2.5 V for 1 min (Fig. 4, gray dots).

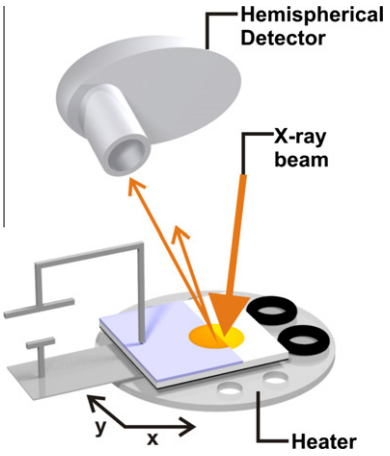

Fig. 2. Experimental setup for the in situ XPS measurements at Elettra synchrotron light facility in Trieste.

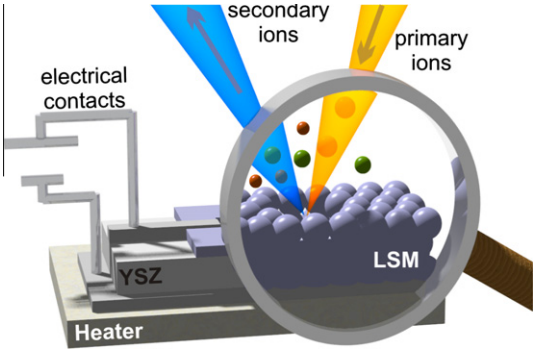

Fig. 3. Experimental setup for the in situ ToF-SIMS measurements.

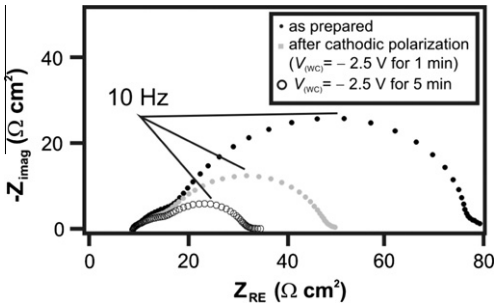

Fig. 4. Impedance spectrum of a freshly prepared LSM electrode (black dots) measured at 800 °C in air and the impedance response of the same electrode after electrochemical activation with a cathodic potential of 2.5 V for 1 min (gray dots) and 5 min (black circles).

Before electrochemical polarization, the impedance was characterized by three overlapping semicircles that correspond to the three elementary steps of the O_2 reduction reaction and the related atomic transport [15]. The low-frequency intercept can be assigned to the oxygen surface exchange reaction consisting of dissociative adsorption of oxygen at the electrode surface, ionization of adsorbed oxygen to O^{2-} ions, and incorporation of oxide ions into the electrode. The mid-frequency part characterizes the oxygen ion transfer processes, mainly diffusion of adsorbed oxygen ions to the TPB. The high-frequency circle contains information on the

charge transfer process and the incorporation of oxide ions into oxygen vacancies of the electrolyte. The shift of the spectrum on the real axis corresponds to the electrolyte resistance.

The observed activation of the electrode saturates with advancing polarization time (Fig. 5a). After 5 min the polarization resistance has already decreased by about 50% of the initial value. Fig. 5b shows that the activation process is composed of two different processes with different time constants. In the first minutes of polarization, a very fast activation process occurs, and after it, a slower activation process is visible.

It is important to note that other studies have already shown that the electrochemical "history" as well as the preparation conditions and thermal treatment strongly influence the impedance response of the electrode [3,10,30–32]. Therefore, the absolute values for the different elements of the equivalent circuit required to fit the electrode impedance are not relevant. We rather focus on the correlation between electrochemical pre-treatment and surface/interface composition and not on the optimization and maximum performance of the electrode system.

The observed impedance under cathodic polarization is in good agreement with the results published by Wang and Jiang [15]. Based on their impedance results, the authors proposed a modified defect model for the explanation of the observed activation, which includes the incorporation of poorly conductive SrO from the surface into the LSM lattice under cathodic polarization. This process is supposed to be fast due to the existence of cation vacancies in the material under SOFC operation conditions and can explain the rapid activation mainly in the first minutes of polarization. A direct evidence for the existence of an insulating layer of SrO on the LSM surface has not been reported in the literature so far. Therefore, we performed in situ XPS and SIMS measurements to investigate the correlation between the observed activation under cathodic current treatment and changes in the surface composition – particularly looking for the Sr signal.

3.1.2. Anodic polarization

Several authors [10,15,30,33] have shown that anodic polarization causes deactivation of the LSM/YSZ electrode characterized by an increase in the impedance response.

Against all expectations, LSM thin-film electrodes show activation in the first minutes of anodic polarization as demonstrated in Fig. 6 and as also reported by La O' et al. [20]. The decrease in the interface resistance and therefore the activation of the thin-film electrodes were accompanied by the formation of blisters and spalling of parts of the LSM film. This increased the TPB length and therefore reduced the polarization. However, we consider this morphological activation of an originally well-covering thin-film electrode not as a real activation, as it is accompanied by serious damage of the film.

After a few minutes of anodic polarization and the initial activation, the expected impedance increase (deactivation) occurs (Fig. 7a). But, both the magnitude of the deactivation and the rate of deactivation are much smaller than the observed activation under cathodic polarization (Fig. 7b).

According to Wang and Jiang [15], the deactivation can be explained by a re-segregation of Sr out of the LSM lattice onto the LSM surface under anodic polarization. The required formation of cation vacancies is energetically unfavorable and therefore a very slow process, which explains the slow de-activation in comparison with the cathodic activation of the electrode.

To clarify to what extent morphological changes contribute to the observed activation/deactivation behavior, TEM and HSEM measurements were performed before and after the electrochemical polarization steps.

3.2. Morphological changes

3.2.1. Cathodic polarization

In addition to the changes of the impedance in terms of activation and deactivation under electrochemical polarization, we also found microstructural and morphological changes after the electrochemical polarization experiments.

A typical HSEM image of a freshly prepared LSM electrode surface is depicted in Fig. 8 (left). The surface is very smooth and dense with a small number of droplets that are typical for the preparation of thin-film electrodes by PLD. After cathodic polarization, the surface morphology had altered, and the formation of distinct grains of submicrometer size with clear grain boundaries was observed (Fig. 8 right). Mizusaki et al. [34] assumed that the formation of grain boundaries is accompanied by the formation of pinholes and therefore an enhanced TPB length which then is the origin for the performance improvement under cathodic polarization. But to act as three-phase boundary, the formed pinholes

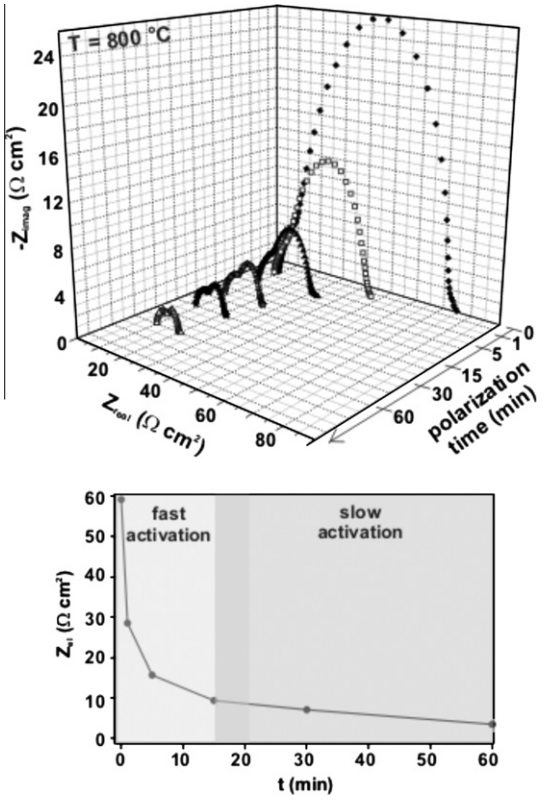

Fig. 5. Impedance response for the LSM/YSZ model electrode under cathodic polarization of 2.5 V for different times (a) and the electrode polarization resistance after different times of cathodic polarization (b).

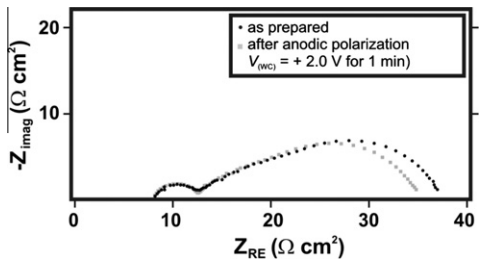

Fig. 6. Impedance spectra of a LSM electrode (black dots) measured at 800 °C and the impedance response of the same electrode after electrochemical activation with an anodic potential of +2.0 V for 1 min (gray dots).

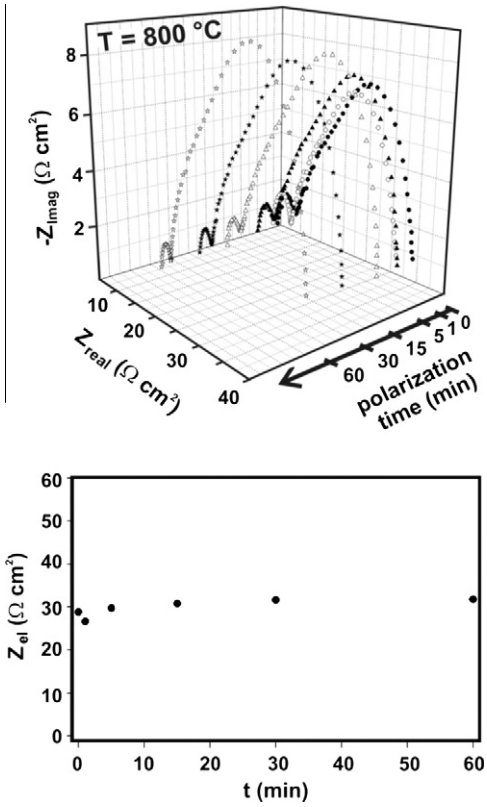

Fig. 7. Impedance response for the oxygen evolution reaction at a LSM model electrode under anodic polarization of +2.0 V for different times (a) and the electrode polarization resistance after different times of anodic polarization (b).

have to extend across the whole film from the surface to the LSM/YSZ interface. To investigate whether such open pinholes form under cathodic polarization, cross-sections of the electrodes before and after electrochemical measurements were studied by TEM.

Fig. 9 shows that both samples exhibit a regular and smooth LSM/YSZ interface. The surface of the as-prepared electrode is plane and smooth with low roughness. In contrast, the surface after cathodic polarization is very rough with distinctive differences in grain size. The formation of nanopores near the interface has occurred under cathodic polarization, but we found no evidence that these holes penetrate the film completely and act as additional TPB, that is, most probably they only form closed pores at the LSM/YSZ interface. However, we cannot exclude that they may act as the origin of interface instabilities in long-term experiments.

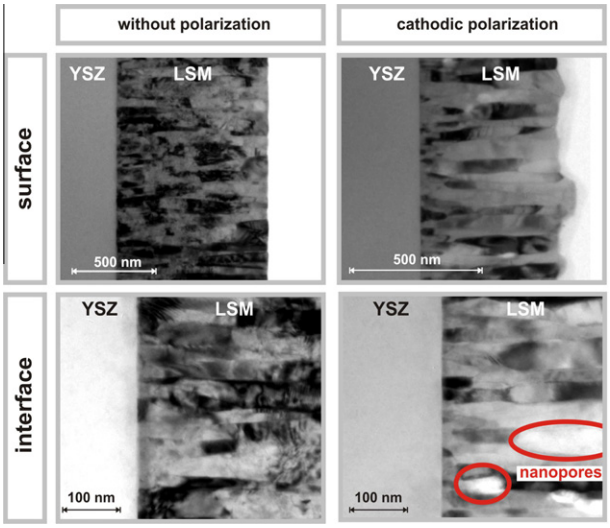

Fig. 9. TEM images of a freshly prepared LSM electrode (left) and the same electrode (right) after cathodic polarization with an applied potential of −2.5 V for 30 min at 600 °C.

3.2.2. Anodic polarization

Anodic polarization causes an increase in the oxygen activity mainly in the vicinity of the TPB. As consequence, the well-adhering thin-film electrode peeled off and small holes of a few micrometer size appeared (Fig. 10). Thus, additional TPB is formed, which results in the observed activation and decrease in the impedance response.

In situ HSEM investigations (Supporting information) show that the formation of pores occurs mainly in the first minutes of anodic polarization which explains that the activation occurs only within the first minutes of anodic polarization, followed by the expected deactivation.

Fig. 11 shows TEM cross-sections of the anodically polarized sample in comparison with the as-prepared electrode. The morphological changes at the electrode surface induced by anodic polarization were similar to those after cathodic polarization. The surface of the electrochemically polarized LSM film became rough, but the changes were less pronounced in comparison with the cathodically polarized sample. In contrast to the electrode after cathodic load, we observed the formation of an impurity phase at the interface of the anodically polarized sample. The amount of this impurity phase is very small, such that the identification in the diffraction pattern was impossible. We hypothesize that this phase originates from the solid-state reaction between LSM and YSZ. Indeed, the formation of a pyrochlore phase ($La_2Zr_2O_7$) between perovskite cathodes and YSZ electrolytes is often reported in the

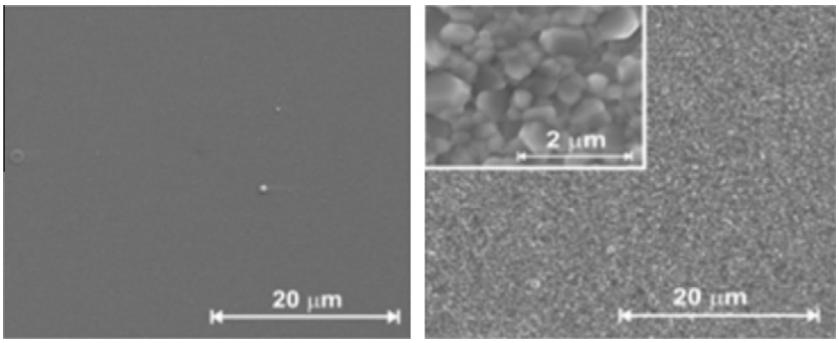

Fig. 8. HSEM image of a freshly prepared LSM electrode (left) and after cathodic polarization (right) with an applied potential of −2.5 V for 30 min at 600 °C.

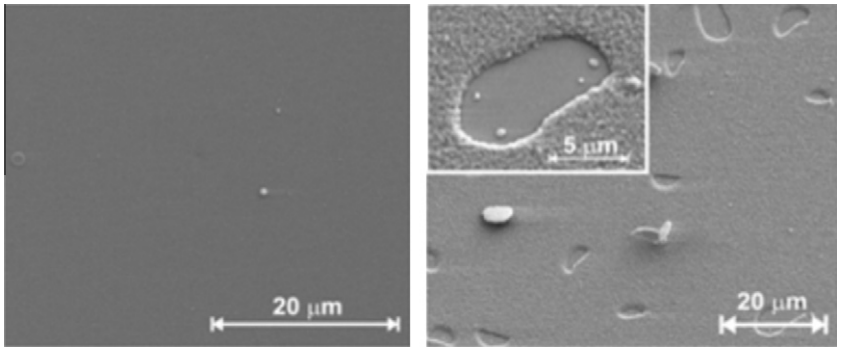

Fig. 10. HSEM image of a freshly prepared LSM electrode (left) and after anodic polarization (right) with an applied potential of +2.0 V for 30 min at 600 °C.

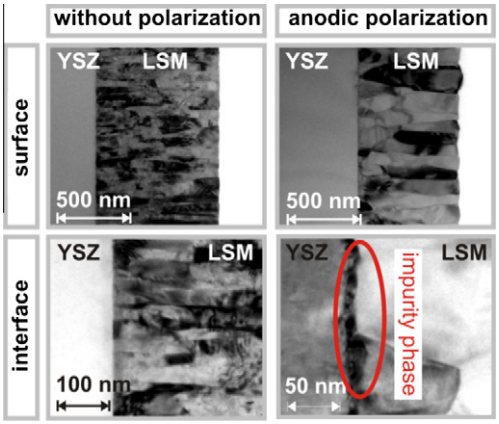

Fig. 11. TEM images of a freshly prepared LSM electrode (left) and the same electrode (right) after anodic polarization with an applied potential of +2.0 V for 30 min at 600 °C.

literature [35,36]. These phases have insulating properties, and the formation reduces the cell performance. Thermodynamic investigations by Yokokawa et al. [36] showed that for the formation of $La_2Zr_2O_7$, oxygen gas is needed in order to facilitate the oxidation of manganese. Under anodic polarization, the oxygen activity increases strongly at the LSM/YSZ interface due to the forced oxygen ion flux from the electrolyte into the electrode. This might be the reason for the formation of the observed impurity phase and can contribute to the measured de-activation under anodic polarization.

The observed changes of the microstructure surely contribute to the observed activation/deactivation under electrochemical polarization, but they can hardly explain the large magnitude of the observed electrochemical activation.

Moreover, electrochemical polarization mainly influences the low-frequency intercept of the impedance response, and therefore, the change of the ORR kinetics is mainly a result of an enhanced surface exchange reaction. Whether surface segregation, which can influence the surface exchange reaction severely, is the reason for the activation of our model electrodes remains an open question if we consider without further analysis. In situ XPS and SIMS measurements were performed in order to obtain more insight into the surface chemistry.

3.3. In situ XPS

The effect of an applied electrical potential on the surface composition of our LSM thin-film electrodes was studied by analyzing the different relative peak areas of the Sr 3d, Mn 3p, La 4d, and Zr 4d lines.

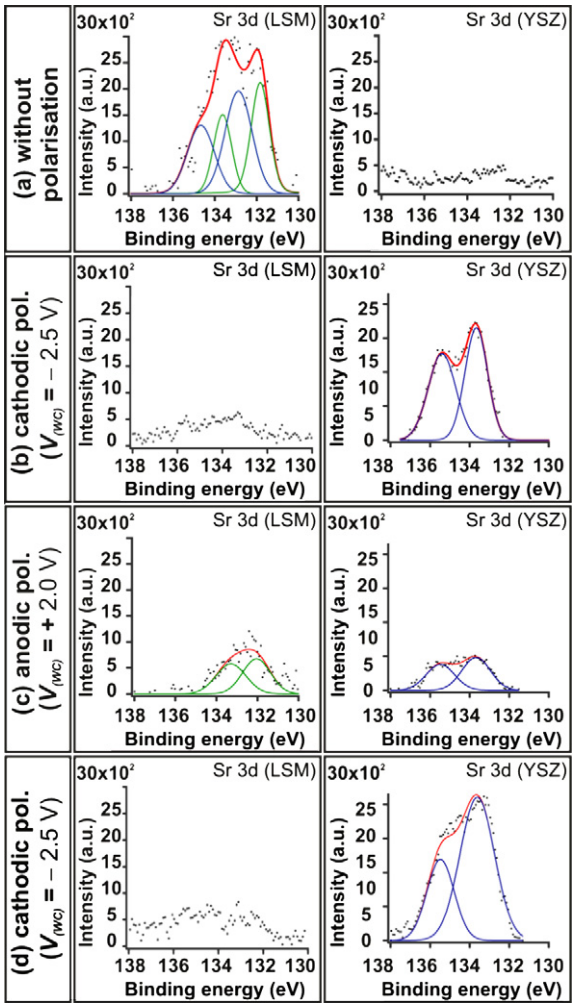

Fig. 12. Sr 3d spectra monitored on the LSM (left) and the YSZ (right) surface with a distance of 50 μm away from the LSM/YSZ interface at 600 °C under the influence of different applied voltages (a) without polarization, (b) −2.5 V, +2.0 V.

3.3.1. Sr 3d

Fig. 12 depicts high-resolution XPS spectra of the Sr 3d peak as a function of different applied voltages, taken at different positions on the LSM and YSZ surface.

Under cathodic polarization, the LSM surface became depleted in Sr. Subsequent anodic polarization lead to a reversible segregation of Sr back onto the LSM surface. A second cathodic step caused again the complete depletion of the electrode surface in Sr.

It is surprising that concomitant to the depletion of the LSM surface in Sr under cathodic polarization, a pronounced Sr 3d peak appears on the YSZ surface. This peak remained clearly visible during the following experiment, so we conclude that the segregation of Sr out of the electrode onto the electrolyte is an irreversible process.

Two components separated by 1.8 eV are required to fit the Sr 3d spectrum. The origin for the additional high-binding energy component (HE) or the so-called "surface core level shift (SCS)" is the existence of a surface species of strontium [37]. The binding energy of this surface state differs from that of Sr in the bulk of the electrode.

This is important to note as the developed component on the YSZ surface shows only the high-binding energy state, and we conclude that only SrO surface species exist on the YSZ.

The total depletion of the LSM surface after cathodic polarization is surprising and implies a non-uniform distribution of Sr to the interface. We suppose that the depletion is a consequence of a voltage profile within the LSM particles due to the ionic-electronic conductivity of the LSM. A SIMS depth profile (see Supporting information) after cathodic polarization shows that the Sr concentration in the volume of the LSM is not uniform with the highest concentration at the interface region between the LSM and YSZ.

The SPEM images (Fig. 13) of the LSM|YSZ TPB region emphasize the diffusion of Sr from the LSM surface into the bulk under cathodic polarization and the corresponding diffusion back under anodic potentials. In the images, bright colors denote high Sr concentrations and dark colors characterize areas with low Sr level.

The SPEM images do not show the development of SrO on the YSZ surface. This can be a result of the experimental approach. The XPS measurements were performed within a distance of 300 μm away from the interface, the SPEM images show only an area of 100 × 100 μm^2 of the YSZ surface. Additionally, the SPEM images were taken during the polarization experiments after all XPS spectra were recorded. Therefore, it is possible that the diffusion front of Sr is visible in the XPS measurement while it is missed in the SPEM images as a result of a too fast diffusion.

Our XPS results also confirm the activation mechanism proposed by Wang and Jiang [15]. We found surface depletion of Sr under cathodic polarization and a reverse segregation under anodic voltages accompanied by the corresponding electrochemical activation or deactivation of the electrode.

3.3.2. Mn 3p

The Mn 3p peak (Fig. 14) appeared as an unresolved doublet and was accompanied by a satellite peak on the high-binding energy side. According to literature, these satellite features are associated with ligand-to-metal charge transfer shake-up transitions [38].

Under cathodic polarization, a complete depletion of the LSM surface in Mn is visible. A reversible diffusion process of Mn back on the LSM surface took place under anodic bias (Fig. 14). But whether Mn only diffuses into the bulk of the electrode or whether Mn also spreads out of the electrode onto the electrolyte surface as suggested by Backhaus-Ricoult et al. [16] cannot be verified unequivocally, as only a small Mn 3p peak appears in the spectra that cannot be separated accurately from the background.

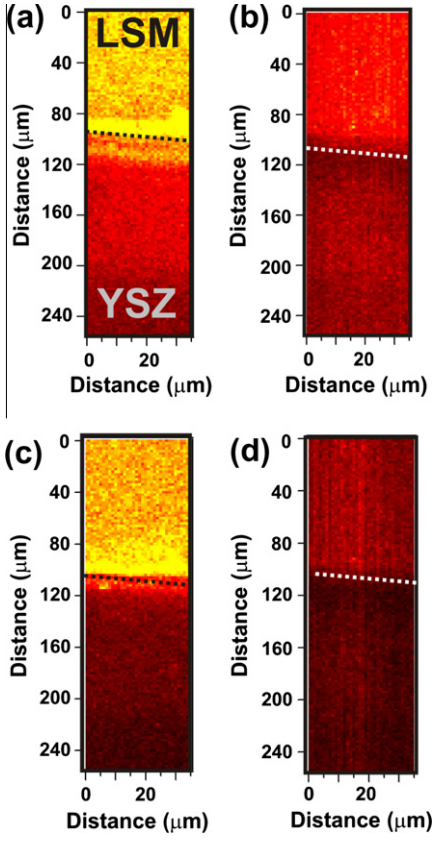

Fig. 13. SPEM images (Sr 3d) of the LSM/YSZ TPB and adjacent LSM and YSZ areas at 600 °C under the influence of different applied voltages (a) without polarization, (b) −2.5 V, +2.0 V.

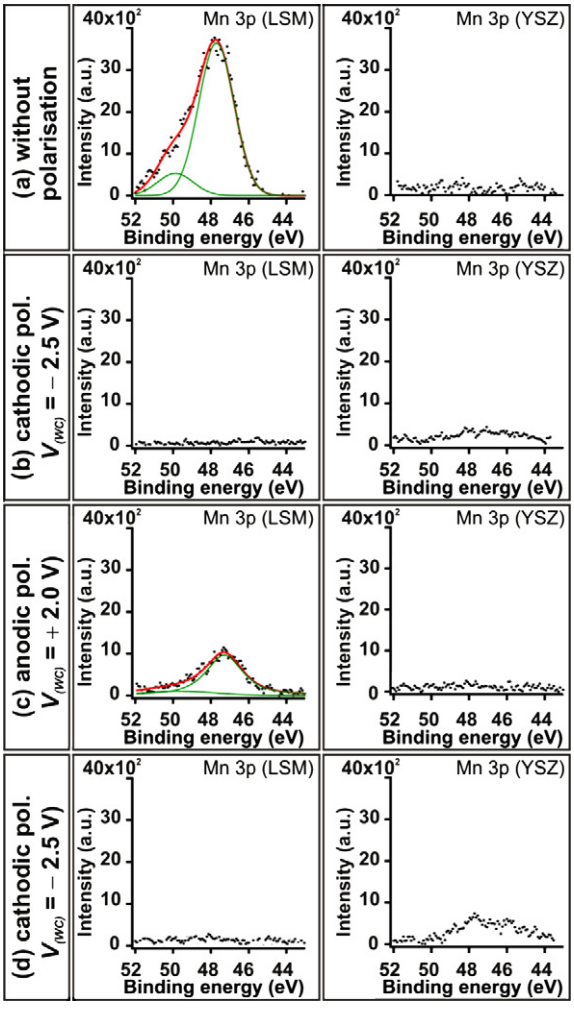

Fig. 14. In situ XPS measurements of the Mn 3p peak under different applied voltages (a) without polarization, (b) −2.5 V, +2.0 V monitored on the LSM (left) and the YSZ surface (right).

In order to use an even more surface-sensitive method, we finally applied in situ SIMS to probe the spreading of Mn onto the electrolyte surface.

It has to be noted that La shows enrichment on the LSM surface under cathodic polarization and depletion during anodic polarization, well corresponding to the segregation/spreading behavior of Sr and Mn (see Supporting information).

3.4. In situ SIMS

SIMS imaging was used as a surface-analytical technique that provides information exclusively on the topmost surface layer, in order to clarify whether Mn diffuses out of the electrode onto the electrolyte as one might conclude from the XPS results.

In the SIMS images, bright colors represent high concentrations of the observed element and dark colors represent low concentrations. The SIMS images were recorded at the TPB between the LSM and the YSZ surface and the adjacent areas.

An enriched surface concentration of manganese at the interface is visible already before electrochemical polarization. (Fig. 15) This is mainly a result of the high-temperature treatment during sample preparation. Under cathodic polarization, the Mn concentration on the electrolyte surface increases with the exception of the first polarization step. Applying an anodic potential causes diffusion back and a concentration increase in Mn on the LSM surface. Hence, the SIMS results confirm that the weak Mn 3p peak on the YSZ in the XPS spectra results from the diffusion of Mn out of the LSM onto the electrolyte.

Our results on the spreading of Mn under cathodic bias from the electrode surface onto the electrolyte support earlier measurements by Backhaus-Ricoult et al. [16] with sintered electrodes. With in situ XPS and SPEM measurements, the authors observed a pronounced spreading of Mn out of the electrode onto the electrolyte by applying a cathodic potential. They concluded that the surface enrichment of Mn(II) ions on the electrolyte is the reason for the electrochemical activation under cathodic polarization, facilitating direct oxygen incorporation at the electrolyte surface. But whether the oxygen ORR can directly occur at the Mn-covered YSZ surface has to be investigated in further studies. The SIMS results for Sr and La support the XPS results (Supporting information).

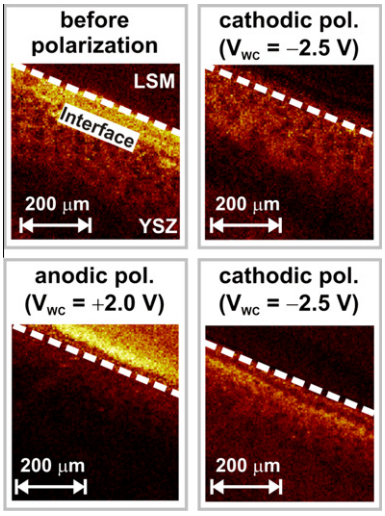

Fig. 15. SIMS images (positive ions) of the Mn surface concentration during an in situ polarization experiment with an oxygen partial pressure of 1×10^{-7} mbar and 550 °C. Each image is normalized by division with the corresponding total ion image. The intensity of the pixels was normalized, such that in all SIMS images of this series, the same color corresponds to the same intensity.

4. General discussion

Our in situ XPS and SIMS results in combination with impedance data prove that the potential-driven surface composition of LSM thin-film electrodes strongly influences the electrode performance.

A performance improvement after electrochemical treatment was often reported for different types of electrodes. Mainly two different causes for the activation are known: (a) the removal of passivating species from the surface of the catalyst/electrode and (b) the generation of an often transient active species, which increases the reaction rate.

An intensively studied system in this respect is the ORR at a platinum (Pt) electrode on yttria-stabilized zirconia (YSZ) as electrolyte. The activation behavior is attributed to the change in the amount of oxygen-containing phases (O–$(Pt)_n$) mainly at the TPB. These phases block the active reaction sites and cause the de-activation of the electrode. Under cathodic polarization, the accumulated PtO_x decomposes and the electrode performance increases [6–8].

Besides the removal of a passivating layer, the generation of an active species is discussed as possible origin for the performance improvement under electrochemical polarization. A typical example for such an activation mechanism is known as NEMCA effect (Non-Faradaic Electrochemical Modification of Catalytic Activity). This effect has been studied intensively for the CO oxidation reaction at Pt/YSZ electrodes. Under electrochemical polarization, the reaction rate for the CO oxidation increases significantly. The commonly accepted but still discussed explanation is that the electrochemical polarization induces the pumping of a catalytic active oxygen species, so-called "spillover" species, onto the electrode surface resulting in an increased reaction rate [39,40].

We relate the observed activation of our LSM thin-film electrodes upon cathodic treatment to a mechanism based on the removal of a passivating surface species, and we propose the following mechanism based on the defect model of Wang and Jiang [15].

The defect chemistry of the LSM phase is characterized by an oxygen nonstoichiometry, meaning that the perovskite phase can exist with oxygen excess and oxygen deficiency (Fig. 16). The changes in oxygen content lead to different defects in the perovskite phase, depending on the oxygen activity.

In the oxygen deficiency region, the formation of oxygen vacancies is compensated by partial reduction of Mn(III) to Mn(II). By transition to the stoichiometric region, the oxygen vacancies are consumed and Mn(II)-ions are re-oxidized to Mn(III). In the oxygen excess region, additional oxygen ions have to be incorporated in the LSM lattice. For $La_{1-x}Sr_xMnO_3$ electrodes, four different mechanisms are discussed to explain the defect chemistry at oxygen excess conditions [41]: (a) the incorporated oxygen ions occupy interstitial sites, (b) the incorporation is accompanied by formation of equal amounts of metal vacancies in both sublattices, (c) the cation vacancies are formed in only one site and the liberated cation migrates to complete the other sublattice forming anti-site defects, (d) cation vacancies are formed in only one lattice accompanied by segregation of these cations out of the lattice. The segregation of cations out of the LSM lattice onto the electrode and electrolyte surface is accompanied by oxidation of Mn(III)-ions.

The defect chemistry has a direct influence on the catalytic activity for the ORR and the cell performance. The formation of oxygen vacancies under oxygen deficiency conditions enhances the oxygen diffusion in the LSM phase and therefore activate the ORR, whereas in the oxygen excess region, the consumption of oxygen vacancies induces a corresponding deactivation. Additionally, the segregation of cations out of the LSM lattice and the formation of cation oxide surface layers onto the electrode surface and TPB

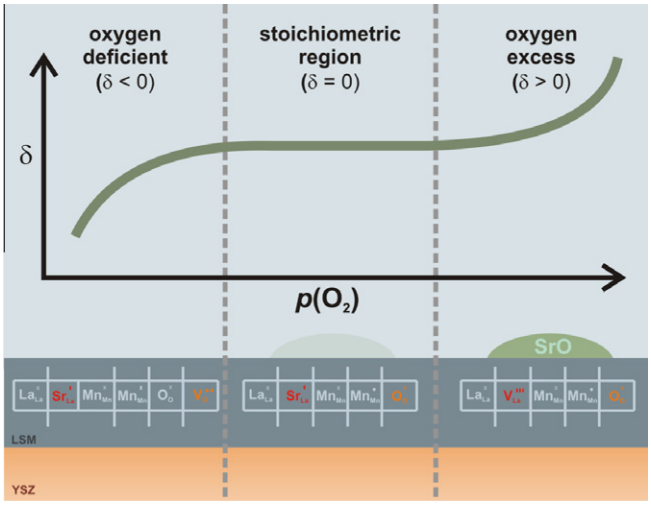

Fig. 16. Schematic diagram of the oxygen stoichiometry of the LSM phase at different oxygen partial pressures and the corresponding defect chemistry.

impede the surface exchange reaction, and a further deactivation is the result.

In our experiments, the freshly prepared electrodes were always annealed at ambient pressure to achieve the perovskite structure. During the annealing process, oxygen is incorporated in the LSM lattice and we detected the formation of SrO on the electrode and electrolyte surface. In conclusion, we propose a defect reaction according to mechanism d). The segregation of Sr out of the LSM lattice onto the electrode and electrolyte surface is accompanied by oxidation of Mn(III)-ions. After the annealing process, the dominant defects in the LSM lattice are probably cation vacancies [42–44] and the LSM phase shows oxygen excess.

By reducing the oxygen partial pressure for the UHV experiments, the LSM phase is still in the oxygen excess region according to the study by Mizusaki et al. [44].

Additionally applying an electrical potential to the electrode, we either increase or decrease the oxygen partial pressure at the electrode and influence the local oxygen activity. As oxygen can be incorporated or excorporated at different locations at the electrode (TPB, interface between YSZ and LSM or on the LSM surface), different local areas may show different oxygen activities. Therefore, we may have local differences in the defect chemistry according to the above-mentioned mechanism (Fig. 17).

Under cathodic polarization, LSM is locally reduced and becomes oxygen deficient. As observed in the XPS and SIMS experiments, the passivating SrO layer on the LSM surface and at the TPB then re-dissolves into the LSM lattice (Eq. (1)) accompanied with the reduction of Mn (Eq. (2)).

This process is supposed to be fast due to the existence of cation vacancies in the material under SOFC operation conditions and can explain the rapid activation in the first minutes of polarization (Fig. 5b).

$$0.8La_{La}^{\times} + 0.2V_{La}^{|||} + 3O_{O}^{\times} + 0.2SrO_{surf} + 0.2V_{O(YSZ)}^{\bullet\bullet} \leftrightarrow 0.8La_{La}^{\times} + 0.2Sr_{La}^{|} + 3O_{O}^{\times} + 0.2O_{O(YSZ)}^{\times} \quad (1)$$

$$0.4Mn_{Mn}^{\times} + 0.6Mn_{Mn}^{\bullet} + 0.2e^{|} \leftrightarrow 0.6Mn_{Mn}^{\times} + 0.4Mn_{Mn}^{\bullet} \quad (2)$$

Further cathodic polarization will lead to the generation of oxygen vacancies (Eq. (3)). As this step is energetically highly unfavorable, it will be relatively slow, which explains the slower activation for the rest of the polarization time (Fig. 5b).

$$0.8La_{La}^{\times} + 0.2Sr_{La}^{|} + 3O_{O}^{\times} + 0.2V_{O(YSZ)}^{\bullet\bullet} \leftrightarrow 0.8La_{La}^{\times} + 0.2Sr_{La}^{|} + 2.8O_{O}^{\times} + 0.2V_{O(LSM)}^{\bullet\bullet} + 0.2O_{O(YSZ)}^{\times} \quad (3)$$

Reversely, under anodic polarization, the oxygen vacancies are consumed (backward reaction of Eq. (3)), followed by re-segregation of SrO at the interface and electrode surface that leads to electrochemical de-activation (backward reaction of Eqs. (1) and (2)).

Our results confirm the defect-based mechanism proposed by Wang and Jiang [15]. We cannot rule out the mechanism based on Mn-spreading onto YSZ according to Backhaus-Ricoult et al. [16], and in principle both effects – SrO segregation and Mn spreading – can occur simultaneously. Backhaus-Ricoult et al. [16] were the first who proposed an activation mechanism for perovskite cathodes with Mn(II) as active species, similar to the activation of Pt electrodes by the spreading of oxygen spillover species as suggested by Vayenas with the NEMCA [39] effect. Under cathodic polarization, the electrolyte surface becomes enriched

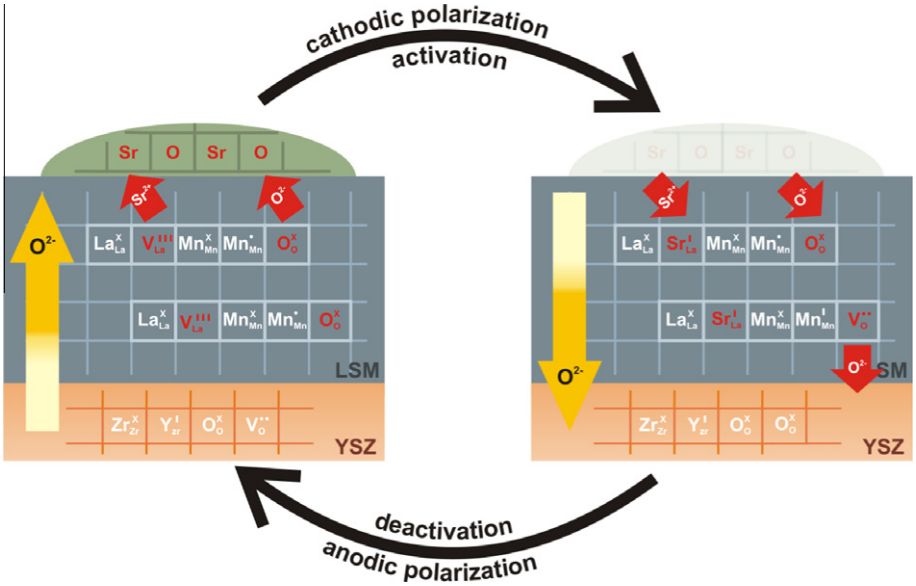

Fig. 17. Defect chemistry of the LSM phase during the electrochemical polarization experiments.

in Mn(II), which may act as catalytically active species. The Mn(II) ions may additionally provide electronic surface conductivity and promote the direct reduction and incorporation of oxygen into the electrolyte. We found small concentrations of Mn on the free YSZ surface, but whether these species really act as catalysts for the direct incorporation of oxygen has to be proven in further studies.

5. Conclusion

Pulsed laser deposition has been shown to be a technique for reproducible preparation of thin-film lanthanum strontium manganite model electrodes that are suited for investigations of surface composition changes. The performance of these LSM thin-film electrodes is strongly dependent upon the applied electrochemical potential. The effect of polarization has been studied on freshly prepared LSM electrodes under different applied electrochemical potentials in air at 800 °C. Under cathodic polarization, a strong activation effect occurs while under anodic polarization a deactivation (after an initial activation) was observed.

Additionally, the polarization treatment has a significant effect on the microstructure of the LSM electrodes. The formation of closed nanopores at the LSM/YSZ interface was observed under cathodic polarization, but we found no evidence that these holes have an influence on the electrochemical performance of the cell. Under anodic polarization, the well-adhering electrode peeled off and additional three-phase boundary is formed, leading to an activation of the cell performance in the first minutes of polarization.

But, the investigated performance changes are mainly a consequence of surface segregation processes and therefore different surface compositions. We analyzed in situ both by X-ray photoelectron spectroscopy and by static secondary ion mass spectrometry an electrochemically induced potential-driven diffusion of different elements at and near the three-phase boundary. Formation of SrO on the cathode surface under anodic polarization and a corresponding removal of SrO from the electrode surface under cathodic polarization indicates that surface Sr species are responsible for the observed activation/deactivation phenomenon. Formation of insulating SrO on the cathode surface inhibits the oxygen reduction reaction and therefore limits the performance of the electrode. Cathodic polarization removes the SrO, while anodic polarization causes its formation.

To get a closer look into the performance of a Solid Oxide Fuel Cell (SOFC) cathode, it is essential to bridge the gap between experimental and real SOFC working conditions. New high-pressure equipments like HP-XPS [45] have to be brought forward to understand the surface changes with electrochemical polarization under real working conditions.

Acknowledgments

Anne-Katrin Huber and Bjoern Luerßen thank the European Union for financial support of their beamtime at sincrotrone ELETTRA within the “VII Framework Program Transnational Access”. This study was otherwise funded by the Justus-Liebig-University. We thank E. Mutoro for helpful comments to the manuscript.

Appendix A. Supplementary material

Supplementary data associated with this article can be found, in the online version, at http://dx.doi.org/10.1016/j.jcat.2012.07.010.

References

[1] N. Minh, N.Q. Minh, Science and Technology of Ceramic Fuel Cells, secon ed., Elsevier Science Ltd., Auflage, 2010. 2.
[2] S. Carter, A. Selcuk, R.J. Chater, J. Kajda, J.A. Kilner, B.C.H. Steele, Solid State Ionics 153 (6) (1992) 597.
[3] S.P. Jiang, J.G. Love, Solid State Ionics 158 (2003) 45.
[4] S. McIntosh, S.B. Adler, J.M. Vohs, R.J. Gorte, Electrochem. Solid State Lett. 7 (2004) A111.
[5] X.J. Chen, S.H. Chan, A. Khor, Solid State Ionics 164 (2003) 17.
[6] S. Sridhar, V. Stancorvski, U.B. Pal, Solid State Ionics 100 (1997) 17.
[7] T. Jacobson, B. Zachau-Christiansen, L. Bay, M.J. Jorgensen, Electrochim. Acta 46 (2001) 1019.
[8] H. Pöpke, E. Mutoro, C. Raiß, B. Luerßen, M. Amati, M.K. Abyaneh, L. Gregoratti, J. Janek, Electrochim. Acta 56 (2011) 10668–10675.
[9] H. Pöpke, E. Mutoro, B. Luerßen, J. Janek, J. Phys. Chem. C 116 (2012) 1912–1920.
[10] Y. Jiang, S. Wang, Y. Zhang, J. Yan, W. Li, J. Electrochem. Soc. 145 (2) (1998) 373.
[11] H.Y. Lee, W.S. Cho, S.M. Oh, H.-D. Wiemhöfer, W. Göpel, J. Electrochem. Soc 142 (1995) 2659.
[12] M. Kuznecov, P. Otschik, P. Obenaus, K. Eichler, W. Schaffrath, Solid State Ionics 157 (2003) 371.
[13] M.J. Jorgensen, P. Holtappels, C.C. Appels, J. Appl. Electrochem. 30 (2000) 411.
[14] S.P. Jiang, J. Sold State Electrochem. 11 (2007) 93.
[15] W. Wang, S.P. Jiang, Solid State Ionics 177 (2006) 1361.
[16] M. Backhaus-Ricoult, K. Adib, T.St. Clair, B. Luerssen, L. Gregoratti, A. Barinov, Solid State Ionics 179 (2008) 891.
[17] H.Y. Lee, W.S. Cho, M. Oh, H.D. Wiemhofer, W. Gopel, J. Electrochem. Soc. 142 (1995) 2659.
[18] M.D. Jong, I. Bergenti, V.A. Dediu, M. Fahlmann, M. Marsi, C. Taliani, Phys. Rev. B. 71 (2005) 014434.
[19] F.S. Baumann, J. Fleig, M. Konuma, U. Starke, H.-U. Habermeier, J. Maler, J. Electrochem. Soc. 152 (2005) A2074.
[20] G.J. La O', R.F. Savinell, Y. Shao-Horn, J. Electrochem. Soc. 156 (6) (2009) 1.
[21] G.J. La O', Y. Shao-Horn, J. Electrochem. Soc. 156 (7) (2009) 1.
[22] A.A. Vance, S. McIntos, J. Electrochem. Soc. 155 (1) (2008) B1–B7.
[23] P. Decorse, G. Caboche, L.-C. Dufour, Solid State Ionics 177 (1999) 161.
[24] Q.-H. Wu, M. Liu, W. Jaegermann, Mater. Lett. 59 (2005) 1480.
[25] M. Nagata, Y. Itoh, H. Iwahara, Solid State Ionics 67 (1994) 215.
[26] J. Rutmann, I. Riess, Solid State Ionics 179 (2008) 108.
[27] M.K. Abyaneh, L. Gregoratti, M. Amati, M. Dalmiglio, M. Kiskinova, J. Surf. Sci. Nanotech. 9 (2011) 158.
[28] M. Marsi, L. Casalis, L. Gregoratti, S. Günther, A. Kolmakov, J. Kovac, D. Lonza, M. Kiskinova, J. Electrochem. Spectrosc. Related Phenom. 84 (1997) 73.
[29] M.L. Casalis, W. Jark, M. Kiskinova, D. Lonza, P. Melpignano, D. Morris, R. Rosei, A. Savoi, A. Abramic, V. Fava, P. Furlan, R. Pugliese, D. Vivoda, G. Sandrin, F.Q. Wei, S. Contarini, L. DeAngelis, G. Gariazzo, P. Nataletti, G.R. Morrison, Rev. Sci. Instrum. 66 (10) (1995) 4870.
[30] P. Jiang, J.P. Zhang, X.G. Zheng, J. Eur. Ceram. Soc. 22 (2002) 361.
[31] J.-D. Kim, G.-D. Kim, J.-W. Moon, Y.-I. Park, W.-H. Lee, K. Kobayashi, M. Nagai, C.-E. Kim, Solid State Ionics 143 (2001) 379.
[32] M.J. Jorgensen, S. Primdahl, M. Mogensen, Electrochim. Acta 44 (1999) 4195–4201.
[33] X.J. Chen, K.A. Khor, S.H. Chan, Solid State Ionics 167 (2004) 379–387.
[34] J. Mizusaki, T. Saito, H. Tagawa, J. Electrochem. Soc. 143 (10) (1996) 3065.
[35] M. Mori, T. Abe, H. Itoh, O. Yamamoto, G.Q. Shen, Y. Takeda, N. Imanishi, Solid State Ionics 123 (1999) 113–119.
[36] H. Yokokawa, N. Sakai, T. Kawada, M. Dokiya, J. Electrochem. Soc. 138 (9) (1991) 2719.
[37] S.W. Han, J.D. Lee, K.H. Kim, H. Song, W.J. Kim, S.J. Kwon, H.G. Lee, C. Hwang, J.I. Jeong, J.S. Kang, J. Korean Phys. Soc. 40 (3) (2002) 501–510.
[38] R.E. van Grieken, Handbook of X-Ray Spectrometry: Methods and Techniques, Marcel Dekker Inc., 1992.
[39] C.G. Vayenas, S. Bebelis, C. Pliangos, S. Brosda, D. Tsiplakides, Electrochemical Activation of Catalysis, Springer-Verlag, 2001.
[40] E. Mutoro, C. Hellwig, B. Luerssen, S. Günther, W.G. Bessler, J. Janek, Phys. Chem. Chem. Phys. 13 (2011) 12798–12807.
[41] N. Grundy, CALPHAD Assessment of the La–Sr–Mn–O System and the Defect Chemistry of (La,Sr)MnO_3 Perovskites used as Solid Oxide Fuel Cell Cathode Materials, Diss. ETH No. 15389.
[42] J. Nowotny, M. Rekas, J. Am. Ceram. Soc. 81 (1998) 67.
[43] F.W. Poulsen, Solid State Ionics 129 (2000) 145.
[44] J. Mizusaki, N. Mori, H. Takai, Y. Yonemura, H. Minamiue, H. Tagawa, M. Dokiya, H. Inaba, K. Naraya, T. Sasamoto, T. Hashimoto, Solid State Ionics 129 (2000) 163.
[45] S.C. DeCaluw, M.E. Grass, C.J. Zhang, F. El Gabaly, H. Bluhm, Z. Liu, G.S. Jackson, A.H. McDaniel, K.F. McCarty, R.L. Farrow, M.A. Linne, Z. Hussain, B.W. Eichhorn, J. Phys. Chem. C 114 (46) (2010) 19853.